Cronfa - Swansea University Open Access Repository

_____

This is an author produced version of a paper published in:
ACS Applied Energy Materials

_____

Cronfa URL for this paper:

http://cronfa.swan.ac.uk/Record/cronfa48051

_____

Paper:

_____

http://www.swansea.ac.uk/library/researchsupport/ris-support/

Designing a high-power sodium-ion battery by *in situ* metal plating

Francesco Mazzali[1,*], Marcin Orzech[1], Arturas Adomkevicius[1,3], Ambra Pisanu[2], Lorenzo Malavasi[2], Davide Deganello[3] and Serena Margadonna[1,*]

[1]Materials Research Centre and SPECIFIC, College of Engineering, Swansea University, SA1 8EN, Swansea, UK

[2]Department of Chemistry and INSTM, University of Pavia, 27100 Pavia, Italy

[3]Welsh Centre for Printing and Coating, College of Engineering, Swansea University, SA1 8EN, Swansea, UK

ABSTRACT: Sodium ion batteries represent a drop-in technology and a more sustainable alternative to Li-ion, but higher energies and power levels are required to meet the demands required by a greener electrification. Here, the design of an anode-free sodium-ion battery is presented and its performances discussed in terms of reduced mass and high power capabilities. The cell consists of an Iron Hexacyanoferrate - reduced Graphene Oxide composite as cathode material whose synthesis is tailored to achieve minimal structural defects (3%) and water content. Its high-potential redox couple $Fe_{LS}(C)$ is stabilized at high rates, granting the full cell with high discharge voltage and power. As negative substrate, a carbon coated aluminum foil was adopted for in situ plating/stripping of Na metal, showing very small voltage hysteresis up to an applied current of 2 mA/cm^2. Overall, this simplified full cell architecture can deliver up to 340 Wh/kg and 500 W/kg at nominal 1C retaining 80% in 250 cycles, with the possibility of delivering 9000 W/kg at 20C. Bridging the boundaries between batteries and supercapacitors, this research aims to expand the range of possible applications for Na-ion technology.

In the context of increased demand for renewable energy, portable electronic devices and electric vehicles, the availability of energy storage systems with high specific energy as well as fast recharging times and specific power has become a global challenge. Much research is currently devoted to the development of pseudo-capacitors and hybrid capacitors with the aim of bridging the gap between high specific energy secondary batteries such as Li-ion-(LIBs) or Na-ion (SIBs) and high-power supercapacitors[1]. However, many of these systems use aqueous electrolytes for fast ion diffusion that limit the working voltage window and therefore specific power. The scientific community is now looking at improving ionic diffusion kinetics through the electrodes and solid electrolyte interfaces to achieve fast re-charging batteries.

A different approach to high specific power and energy could be to re-think the full cell architecture. For instance, a new concept of "anode-free" metal plating battery has been demonstrated for both LIBs[2] and SIBs[3], where plating/stripping is carried out *in situ* on a substrate during operation of the battery. In this configuration the source of ions is the cathode material, while the anode is just a current collector. Qian et al.[2] firstly demonstrated this concept on a Cu//LiFePO$_4$ system, highlighting that replacing the graphite anode with a copper substrate potentially increases the energy density by 50%. The same concept, applied by Cohn et al.[3] on a sodium system, shows that ~400 Wh/kg (almost double the

value of conventional SIBs) can be obtained pairing a carbon coated aluminum foil and a Na$_{1.5}$FeS$_2$ cathode. The high specific energy can be coupled with fast charging/recharging time as adoption of this simplified "anode-free" architecture circumvents the problem associated with the slow kinetics of intercalation into a bulk anode material (such as hard carbon that suffers from deteriorating electrochemical properties with increasing current rates[4]) by taking advantage of the faster surface-based mechanism of plating/stripping. Indeed, our investigation of the performances of a carbon coated aluminum foil, as substrate for sodium plating and stripping in two different ether-based electrolytes at high current rates, showed low values of overpotential and average plating hysteresis up to 2 mA/cm^2. These results confirm the suitability of this substrate for the design of a high-rate system. To take advantage of the fast kinetics associated with Na electroplating, a suitable high capacity cathode material that performs efficiently at equivalent high current rates and working at a high average potential needs to be employed. During the last decades, a plethora of cathode materials for SIBs have been synthetized and tested. Among them, those based on Prussian blue analogues (PBAs) have attracted tremendous interest for their high theoretical specific capacity as well as fast kinetics and superior rate capabilities[5]. These attractive properties result from their 3D open framework structure that allows facile intercalation/deintercalation of Na ions as well as being able to ac-

commodate large volume changes while maintaining its structural integrity. Iron hexacynoferrate (Fe-HCF) has been identified as one of the most promising cathode material for sodium ion batteries as it can undergo a two one-electrode redox process to afford sodium iron hexacyanoferrate $Na_2Fe[Fe(CN)_6]$ resulting in high theoretical specific capacity. However, it suffers from low cycling stability, low coulombic efficiencies and undesired side reactions with organic electrolytes as well as poor electronic conductivity. These limitations have been addressed following different strategies. In particular, nanostructuring and optimized synthetic procedures have been proven to be effective in limiting defects in the crystal structure (e.g. number of $[Fe(CN)_6]$ vacancies and coordinated water) that are considered the main cause for the poor electrochemical performances[6,7]. Also, the fabrication of PBAs composites with carbonaceous materials such as reduced graphene oxide[8,9], graphene oxide[10], ketjen black[11] and carbon nanotubes[12] has been successful employed to inhibit particle growth during synthesis, improve interparticle electrical conductivity and protect Fe-HCF from undesired reaction with the electrolyte. It has been shown that the use of submicron cubes of Fe-HCF coated by polypyrrole[13] is effective in improving cycle and rate performance. Quite outstanding are also the performances reported for a Fe-HCF@carbon composite that showed a stable capacity of 90 mAh/g after 2000 cycles at 20C[11]. Wrapping of Fe-HCF nanospheres into graphene rolls reduces side reactions leading to a stable capacity of 110 mAh/g and high capacity retention over extended cycling. Similarly, a sodium Fe-HCF -reduced graphene oxide composite showed an initial discharge capacity of 149.7 mAh/g at 200 mA/g and a capacity retention of 91.9% after 500 cycles at the same current rate[8]. The outstanding electrochemical performances are generally explained in terms of absence of coordinated water which leads to a full utilization of the Fe^{II}-Fe^{III} redox couples.

From all these results it is evident that PBAs based materials are ideal candidates to realize high-power and high-energy SIBs. Our aim was to fabricate such system by taking advantage of the simplified cell architecture and fast kinetics offered by the "anode-free" concept. We, therefore, opted to synthesize a carbon composite of Fe-HCF with low vacancies and water content as cathode material. For this purpose, we employed procedures already established and used reduced graphene oxide (rGO) as a template for reducing particle growth and amount of crystal vacancies as well as providing a highly conductive matrix. To understand the effect of rGO, bare Fe-HCF samples were also prepared using PVP for particle confinement as to achieve comparable particle size. The best performing cathode material was then coupled with a carbon coated aluminium foil (CB/Al) as substrate for Na plating and stripping. An ether based electrolyte has been chosen as many recent studies proved that it is the most suitable for a stable, uniform and conductive SEI layer on sodium metal anodes at room temperature and enables stable and reversible utilization of stripping/plating mechanisms[14].

The so designed full cell delivered 115 mAh/g and retained 79% of capacity after 250 cycles at nominal rate of 1C, with an average discharge potential of 2.98 V. Due to the good crystallinity of the lattice and the enhanced electron conductivity, the high potential Fe^{II}-Fe^{III} redox couple showed remarkable capability at high current rates. The Fe-HCF@rGO//CB/Al system is able to deliver a specific energy of 338 Wh/kg at 1C while maintaining a specific power of 503 W/kg or delivering 9010 W/kg when the current rate is increased to 20C.

This work highlights the importance of a material design oriented towards real world full cell application, where matching positive and negative electrode determines the specific energy and power of the battery system. A simplified architecture of anode-free full cell is achieved and its promising performances tested under a range of rates, proving to be a highly competitive and inexpensive approach for future sodium ion batteries.

Experimental methods

Material synthesis

For the synthesis of the composite Prussian Blue material Fe-HCF@rGO, first a dispersion of rGO in water is prepared, 0.05 g of as received Reduced Graphene Oxide powder (M921, Ossila Ltd.) were added to 100 mL of deionized water, the solution was ultrasonicated with probe for 2h, with a total energy input of 100kJ. The obtained dispersion was then stirred and 22.5 mmol of HCl (37 %wt) and 1.25 mmol of $Na_4Fe^{II}(CN)_6$ were added as the only iron source. The solution was transferred into a round bottom flask and immersed into a silicon oil bath kept at 175 °C, to achieve a reflux temperature of 100 °C. After stirring vigorously for 4h the solution was cooled down to RT and then filtered and washed with deionized water and acetone few times. The obtained powder was fully dried in vacuum oven at 60°C overnight. Considering a yield from $Na_4Fe(CN)_6$ into PB of around 33% (as obtained by analogous synthesis without rGO), the mass ratio PB:rGO is around 80:20 %wt.

To investigate the effect of rGO, a bare Prussian Blue (Fe-HCF) with similar particle size and similar lattice constants was synthesized. Firstly, 1.6 g of PVP were stirred in 100 mL of distilled water. 1 mL HCl (37 %wt conc.) and 0.484 g of $Na_4Fe(CN)_6$ were added and stirred until complete dissolution. The solution was transferred and sealed into a PTFE lined autoclave vessel before being heated up to 80°C for 17 h. After natural cool down to RT the product was collected by centrifuging in deionized water and acetone few times, and then fully dried in vacuum oven at 60°C overnight.

Both materials were further dried at 210°C under high vacuum of 10^{-6} bar overnight. This treatment resulted in the removal of most interstitial water in the case of the Fe-HCF@rGO composite while maintaining its structural integrity. However, for the bare Fe-HCF, the same procedure induces structural degradation and amorphization. The electrochemical testing was therefore always performed on the high vacuum dried Fe-HCF@rGO and the vacuum oven dried Fe-HCF.

Material characterization

X-ray powder diffraction (XRD) patterns of the as synthetized materials were measured in transmission with a Bruker D8 Advance diffractometer mounting a Cu Kα radiation source ($\lambda = 1.5406$ Å). The XRD patterns were collected over the range 10–80° by keeping the step size of 0.015° at a scan rate of 6 s per step.

Thermo Gravimetrical Analysis (TGA) was conducted under Nitrogen atmosphere on a Perkin Elmer STA instrument, with a step of 10°C/min up to 500°C.

For electron microscopy, a JEOL 7800F FEG SEM was used, while for EDX analysis, Zeiss EVO SEM was used. Powder samples were sputter-coated with 10 nm of Au/Pd. The EDX results were averaged over three different sites and Oxford software suite was used for fitting. Optical images were acquired with SmartZoom Zeiss microscope at a magnification of 500x.

Electrochemical evaluation

Positive electrodes of Fe-HCF@rGO and bare Fe-HCF were prepared by mixing the active powder with Carbon Black Super-P (Timcal) and PVDF KynarFlex 2801 (Arkema, France) in a ratio of 80:10:10 in THF. All performances reported here consider only the mass of PB (not rGO) as the active material. Slurries were casted on aluminum foil and punched into discs of 12.5 mm diameter before being dried under vacuum and transferred into Ar filled glovebox ($H_2O < 0.5$ ppm and $O_2 < 0.5$ ppm). CR2032 coin cells were assembled using Na discs as counter/reference electrode and Whatman Glassfiber GF/D as separator. After assembling 6 to 8 hours of rest are allowed for proper wetting of electrodes and potential stabilization. Galvanostatic cycling was conducted on Maccor (USA) and VMP3 (BioLogic, France) at room temperature.

The negative substrates were prepared by mixing Carbon Black and CMC 90:10 %wt in water:ethanol 1:1 v/v, and the resulting slurry was casted as very thin layer on aluminum foil. The uniform and light mass loading was 87 ug/cm^2.

For half-cell and full cell evaluations, 1 M NaPF$_6$ (FluoroChem) in Diglyme (a.k.a. DGDME or G2) (Acros Organic) was used as electrolyte. The NaPF$_6$ salt was fully dried at 150 °C for 20 h under Ar before use. For full cell evaluations, Celgard trilayer was used as separator.

Prior full cell tests, cathode and negative substrate were separately preactivated in half cell against sodium for 5 cycles, disassembled at their maximum state of sodiation, and reassembled in full cell. In the full cell configurations. the positive electrodes have a mass loading of 1.5 mg/cm^2. A current of 150 mA/g (1C) is applied, corresponding to 0.23 mA/cm^2, which is the aerial current density at which the substrate is subjected.

Results and Discussion
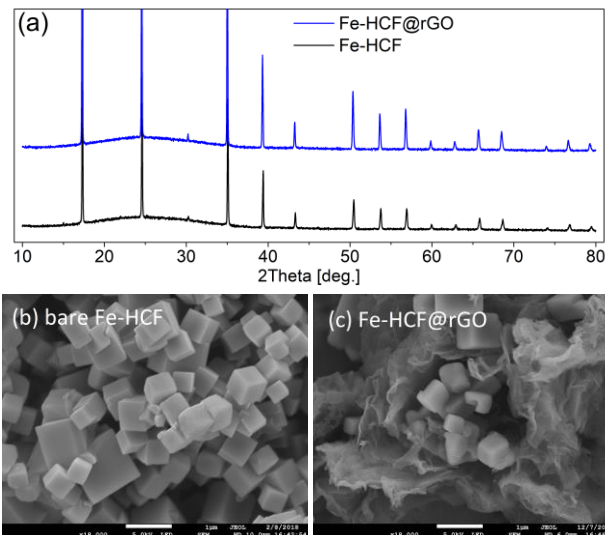
Characterization of the cathode materials

Figure 1. Comparison of X-ray powder diffraction profiles of bare Fe-HCF and Fe-HCF@rGO (a). SEM images for bare Fe-HCF (b) and Fe-HCF@rGO (c); scale bar 1μm.

The room temperature powder diffraction profiles of bare Fe-HCF and of the composite Fe-HCF@rGO (Figure 1(a)) can be readily indexed with the characteristic face centred cubic structure (space group *Fm-3m*) adopted by many Prussian blue analogues with general formula $A_xM^a[M^b(CN)_6]_y \cdot \square_{1-y} \cdot zH_2O$ (where A=alkali metal, M^a and M^b =first raw transition metals, $\square$=vacancies of [$M^b(CN)_6$]). In order to highlight and study the change in electrochemical performances introduced only by the rGO matrix, the two materials were selected as to have comparable composition and therefore lattice dimensions. From the Rietveld refinement (see SI for more details) the obtained lattice constants are a =10.25003(4) Å for Fe-HCF@rGO and a =10.23061(6) Å for Fe-HCF. No evidence of secondary spurious phases is found. Much work has been devoted in the past to the detailed characterization of the structural and electronic properties of iron- hexacyanoferrate adopting the face-centred cubic structure[15,16]. The crystal structure can be described as a three-dimensional network of Fe(NC)$_6$ and Fe(CN)$_6$ octahedra linked by the CN ligands. The Fe(CN)$_6$ vacant positions are replaced by H$_2$O molecules completing the coordination sphere of neighbouring Fe(NC)$_6$ cations while the Na$^+$ ions are disordered in the tetrahedral interstices of the framework structure. Infrared and Mossbauer spectroscopy have been extensively used to determine the Fe valence states and all techniques confirmed the assignment Fe^{II}-CN-Fe^{III} [15,16]. According to ligand field theory, the Fe^{III} that is linked to the N side of the cyanide bridge is in its high spin state (Fe$_{HS}$(N)) while the Fe^{II} bonded to the C is in the low spin electronic configuration (Fe$_{LS}$(C)).

Energy dispersive X-ray spectroscopy (EDX), and thermogravimetric analysis (TGA) were employed to estimate the chemical composition of both samples which resulted to be $Na_{0.90}Fe^{III}[Fe^{II}(CN)_6]_{0.97}\cdot\square_{0.03}\cdot2.48H_2O$ for Fe-HCF @rGO and $Na_{0.53}Fe^{III}[Fe^{II}(CN)_6]_{0.88}\cdot\square_{0.12}\cdot2.31H_2O$ for bare Fe-HCF (refer to SI for more details). In accordance with previous studies the composite shows a reduced number of structural defects and higher sodium content as compared to the bare sample (3% vacancies against 12%). Defects translate directly into a limitation of the maximum storage capacity which can be obtained from these materials. The first discharge capacity expected for these materials (based on the wet mass) is 48.2 mAh/g for Fe-HCF and 73.6 mAh/g for Fe-HCF@rGO, while the maximum capacity obtainable is 128.5 mAh/g, and 145.2 mAh/g respectively.

The water present in the crystal structure plays a major role in the electrochemical performance of Fe-HCF. It is well known that PBA materials can incorporate two types of water, coordinated and interstitial (or zeolitic) water. The coordinated water occupies the $[Fe(CN)_6]$ vacancies in the form of $(H_2O)_6$ clusters, coordinating with the Fe(II) of $Fe_{LS}(C)$ sites to maintain the electroneutrality[8,17]. On the other hand, interstitial water is physically adsorbed into the A-sites and can be removed without affecting the integrity of the framework structure. The absence of interstitial water is crucial for the long term electrochemical stability as side reactions at high potentials in fluorinated organic electrolytes are avoided. In the as synthesized Fe-HCF@rGO composite, due to the low vacancies content, the water is mostly interstitial, and can be removed through drying processes under high vacuum. As confirmed by previous work, the structure of Fe-HCF does not incur in decomposition at least up to ~220 °C[8,18], and it's only around 300°C that the release of $(C\equiv N)_2$ is detected[9] in the TGA. Hence, the prepared electrodes were dried at 210°C under high vacuum of 10^{-6} bar overnight. The XRD profile of the dried composite is reported in Figure S3, in comparison with the pristine material. A small shift towards smaller lattice constants can be noticed for the dried sample (a=10.1992(3) Å) as would be expected from the removal of interstitial water. The diffraction profile also shows the presence of a small amount (2%) of a rhombohedral phase which has been previously reported for Na-rich and vacancies/water free sodium iron hexacyanoferrates[16,19]. The appearance of this secondary phase implies that the actual composition is locally inhomogeneous in the original sample but clearly demonstrates the effective removal of interstitial water from the as prepared Fe-HCF@rGO. Indeed, TGA analysis confirmed a reduced water content to $Na_{0.90}Fe^{III}[Fe^{II}(CN)_6]_{0.97}\cdot\square_{0.03}\cdot0.48H_2O$. The dried material is expected to deliver in first discharge 82.7 mAh/g, and reaching maximum capacity of 162 mAh/g. An analogous drying treatment was not possible on bare Fe-HCF as it resulted in structural degradation. This is because most of the water is sixfold coordinated within the vacancies sites and their removal induces collapse of the framework structure.

The two samples (bare Fe-HCF and Fe-HCF@rGO) were tailored to have similar particle size. The relative SEM images are shown in Figure 1b-c. The bare Fe-HCF shows a broadly homogeneous cubic shape with edge length of about 500 nm on average. Larger cubes with edges up to 1 μm are also sporadically observed. Similar morphology and particle size are also observed in the composite. The rGO does not coat or cover the Fe-HCF submicron cubes but provides the ideal matrix for distributed nucleation and uniform growth of the Fe-HCF crystals which, in turn, are in intimate contact with a highly conductive backbone. The effect of the rGO in the confinement of the size is illustrated in Figure S5, where a control synthesis of Fe-HCF without rGO (and without PVP) is reported. In this case, cubic shaped particles with side length > 1μm are produced which is double the average size of those obtained in Fe-HCF@rGO.
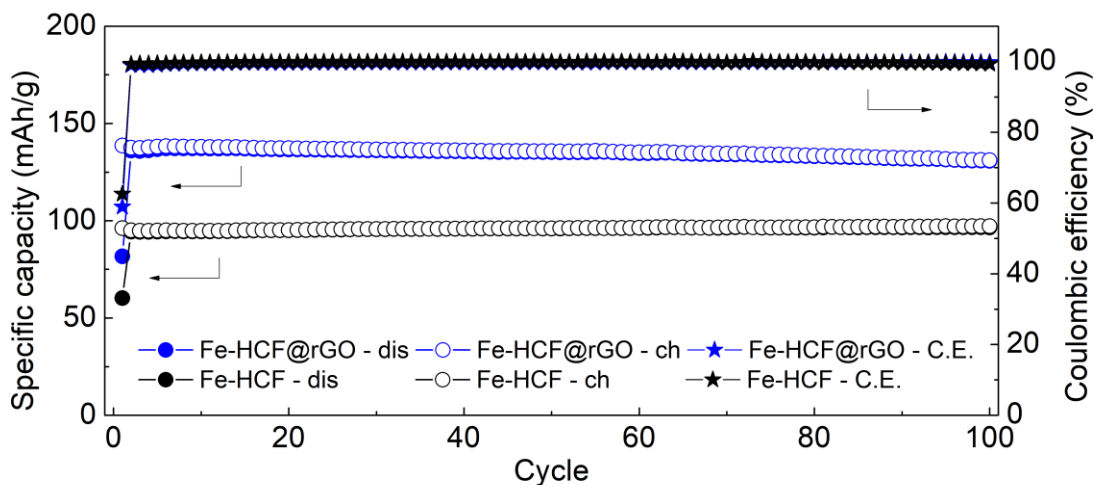

Figure 2. Long cycling performance in half cell of bare Fe-HCF (black) and Fe-HCF@rGO (blue) over 100 cycles at 75 mA/g in 1M $NaPF_6$/G2.

Cathode materials electrochemical performances

The electrochemical performance of bare Fe-HCF and Fe-HCF@rGO was evaluated through galvanostatic charge/discharge cycling in the voltage window 2.0-3.9 V at different current rates. It should be noted that all tests were performed on the high-vacuum dried composite Fe-HCF@rGO and on the oven dried material in the case of bare Fe-HCF. Electrolyte formulation is a key factor that determines the SEI stability of sodium metal electrode. Carbonate and ether based electrolytes have been extensively studied, with the latter showing better performance in terms of plating/stripping reversibility and SEI firmness[14,19].

For this reason, the electrochemical tests on both materials were all performed using a 1 M NaPF$_6$ in Diglyme as electrolyte. Fe-HCF@rGO and bare Fe-HCF showed a first discharge capacity of 81.7 and 60.2 mAh/g, respectively, at the current rate of 75 mA/g (Figure 2). The values obtained are in line with the maximum discharge capacity calculated based on the original Na concentration and number of vacancies and prove an almost full utilization of the active material.

The first discharge curve of both materials shows two plateaus at 3.3 and 2.9 V that correspond to the Fe(III)/Fe(II) redox energies of the Fe$_{LS}$(C) and Fe$_{HS}$(N) octahedra, respectively. In comparison with the bare Fe-HCF, the rGO composite shows much flatter and well defined plateaus with both redox couples providing a larger contribution to the total capacity. This behaviour is maintained upon cycling with reversibility. Both samples show a very high coulombic efficiency of 99.3% for Fe-HCF and 98.9% for Fe-HCF@rGO at the second cycle, increasing along cycling up to 99.8% for both samples. This high efficiency grants a very good capacity retention of 95.5% for the composite and 99% for the bare Fe-HCF over 100 cycles. The slight difference in retention could be ascribed to a more complex Cathode Electrolyte Interphase (CEI) arising from the presence of the carbon matrix. Despite this, Fe-HCF@rGO showed a much higher value of capacity (+30%), proving the effect of the template synthesis on the electrochemical performance. These remarkable performances confirm the suitability of Prussian Blue materials for high-performance full cell applications.
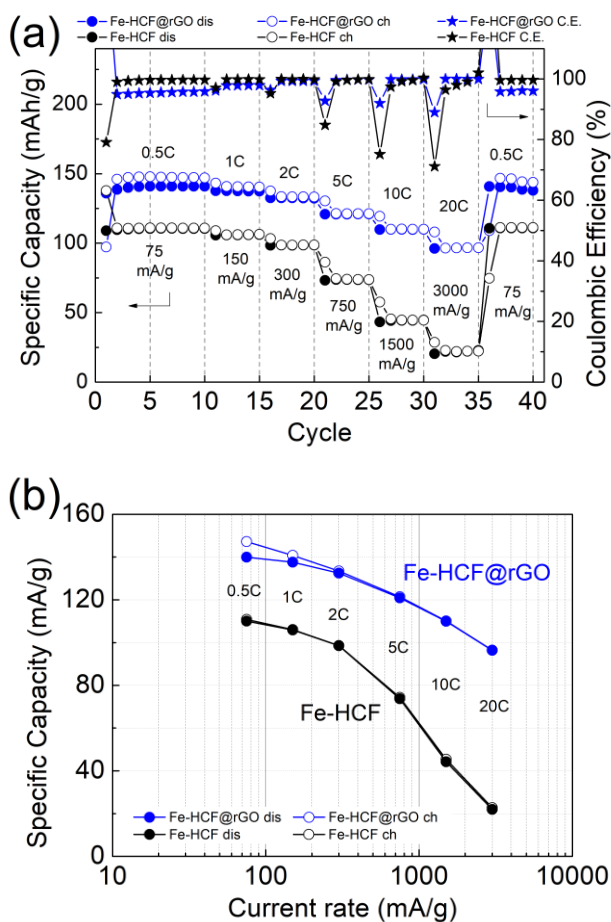

Figure 3. Rate capability tests in half cell. Waterfall plot of charge/discharge capacities and efficiency at various C rates for Fe-HCF (black) and Fe-HCF@rGO (blue) (a) and their representation against current rate in semilog plot (b).
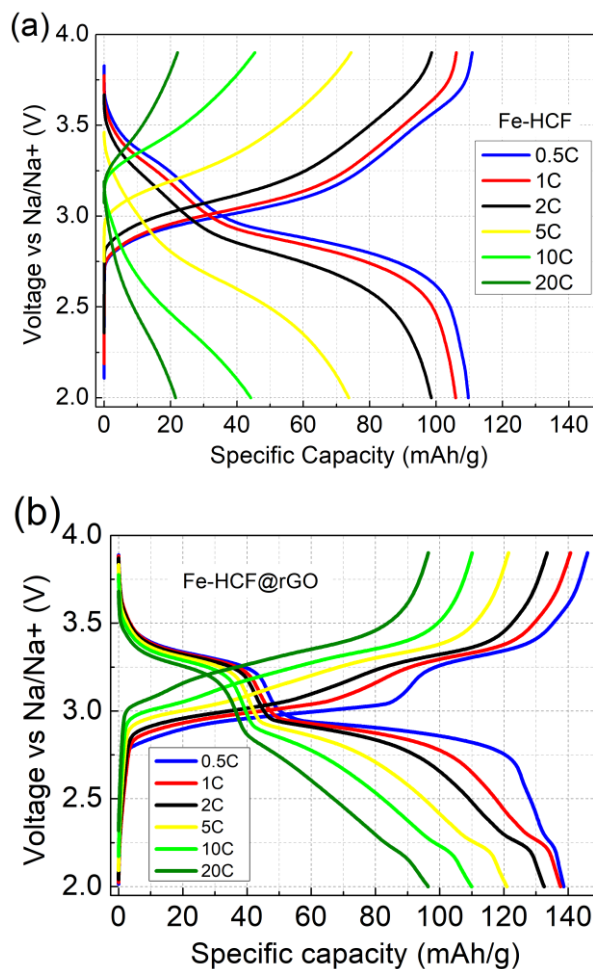

Figure 4. Charge/Discharge voltage profiles at increasing C-rate for bare Fe-HCF (a) and Fe-HCF@rGO (b). All tests in 1M NaPF$_6$/G2.

Rate capability measurements were also performed to further determine the suitability of the materials as cathodes for high power "anode-free" full cell architecture. The resulting charge/discharge capacity versus cycle number plot is presented on Figure 3. Average discharge capacities for Fe-HCF@rGO are 140, 138, 133, 121, 110 and 96 mAh/g, and for bare Fe-HCF 110, 106, 99, 74, 44 and 21 mAh/g, obtained at current rate of 75, 150, 300, 750, 1500 and 3000 mA/g, respectively (see Figure 4). At the highest current rate measured, Fe-HCF@rGO maintains 69% of its capacity while for bare Fe-HCF only 19% is retained. After deep cycling at 3000 mA/g, when the current rate is set back to 75 mA/g, both materials recovered the initial discharge capacity of 140 mAh/g and 110 mAh/g, respectively. Long cycling of Fe-HCF@rGO at 10C over 100 cycles is also reported in Figure S7. The rate capabilities displayed by the Fe-HCF@rGO composite are superior not only to the bare Fe-HCF presented in this work but also to many other similar materials including Fe-HCF nanospheres wrapped in graphene sheets[20] (capacity retention at 10C of about 72%) and rGO-coated Fe-HCF nanoparticles which shows an average discharge capacity of 112 mAh/g at 800 mA/g[8]. However, even faster reaction kinetics then Fe-HCF@rGO have been reported for a Fe-HCF/carbon powder composite with lower initial Na content, higher levels of vacancies and interstitial water. This material achieved 77.5 mAh/g at 90 C and enhanced cycling stability[11].

These outstanding performances were ascribed to the fast reaction kinetics of the low voltage $Fe_{HS}(N)$ redox center which relies on the Na insertion to enhance electron conduction. A different behavior is observed in the case of Fe-HCF@rGO where increasing the current rate results in the shortening of the low voltage plateau that also becomes much less defined as compared to the high voltage plateau related to the $Fe_{LS}(C)$ octahedra. This points towards a scenario were the $Fe_{HS}(N)$ redox centers show slower kinetics causing a greater capacity loss than the $Fe_{LS}(C)$. An opposite behavior is instead displayed by bare Fe-HCF were the $Fe_{LS}(C)$ octahedra show higher rate of decline in agreement with what has been reported for most Fe-HCF based materials.

The observation of fast rates of reaction for the $Fe_{LS}(C)$ octahedra in Fe-HCF@rGO is quite significant. A number of efforts have been reported to increase its redox response including reduction of vacancies and water. For instance, it has been shown that in the dehydrated Fe-HCF, which adopts a rhombohedral structure with very few vacancies and high sodium content, the $Fe_{HS}(N)$ octahedra have a higher rate of decline than that observed for the $Fe_{LS}(C)$ redox centers as their electron filling is less energetically favored[21]. Furthermore, in this system the electrons are highly itinerant contributing to enhanced electrical conductivity and rate performance. Our Fe-HCF@rGO displays a similar behavior as can be deduced by plotting the first derivatives of the charge vs voltage curves obtained at current rates of 75 mA/g and 750 mA/g and comparing them with those obtained for bare Fe-HCF (Figure 5). For the latter, when the current rate is increased, a polarization of 0.2 V during oxidation and of 0.26 V during reduction can be observed for the $Fe_{HS}(N)$ couple (Figure 5a). On the other hand, for the rGO composite these values of polarization are drastically reduced to 0.02 V during oxidation and 0.04 V during reduction (Figure 5b). Moreover, no polarization is observed for the $Fe_{LS}(C)$ octahedra in the case of Fe-HCF@rGO. This behavior highlights that the redox activity of the high voltage $Fe_{LS}(C)$ is maintained at high current rates with no polarization in agreement with what has been reported for dehydrated Fe-HCF. It would appear that the removal of interstitial water, as well as a higher Na content, are key to increase the redox response at high voltage. In the Fe-HCF@rGO composite these characteristics are coupled with the enhanced electron conductivity provided by the rGO matrix, which allows good adaptability to higher current rates.

The electrochemical footprint of the carbon matrix is also visible in Figure 4b and 5b, where a low intensity peak is visible at around 2.25 V. This feature is absent in the voltage profile of the bare Fe-HCF and therefore can be attributed to the reduction of rGO. Previous work on GO and rGO in Li-based electrolytes suggests that the reduction of functional groups on the rGO can occur between 1.8 to 2.6 V vs Li/Li^+ (1.47 to 2.27 V vs Na/Na^+), while the oxidation occurs at much higher potentials, between 3 and 4 V vs Li/Li^+ (2.67 and 3.67 V vs Na/Na^+)[22–24]. For Fe-HCF@rGO, the oxidation peak is likely overlapped with the stronger oxidation peak of $Fe_{HS}(N)$, as it can be seen in Figure 5b from the light shoulder around 2.85 V. Despite not contributing significantly to the storage capacity, the rGO matrix plays a pivotal role in facilitating the electron exchange, which turns into a reduced polarization upon increasing the current rate. The sharpness of the redox peaks for Fe-HCF@rGO compared to Fe-HCF is also a confirmation of enhanced electron transfer.
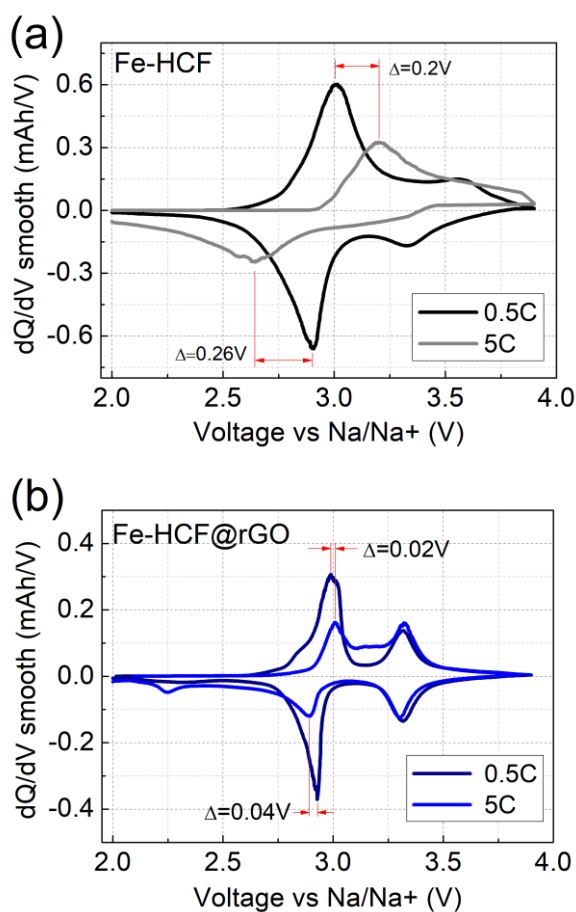
Figure 5. Comparison of voltage derivatives of the specific capacity vs voltage curves obtained at 0.5 C (75 mA/g) and 5 C (750 mA/g) for bare Fe-HCF (a) and Fe-HCF@rGO (b).

Anode-free full cell electrochemical performances

Plating and stripping of Na metal on an ad-hoc designed substrate (that also functions as current collector) has been proven to be highly stable and efficient at high currents opening the way to the assembly of high-power and high-energy systems. Many different substrates have been recently reported in the literature. Among these, a carbon coated aluminum current collector appears to be an effective and cheap choice. The thin carbon coating with a negligible mass (87 μg/cm^2) is able to lower the nucleation overpotential during sodium seeding and to increase the uniformity of plating/stripping, reducing the risk of Na dendrite formation[3]. These characteristics are very appealing when considering the very limited amount of sodium that would be present in a full cell setting. The beneficial effects of the carbon layer can be better understood from the electroplating tests performed on a pure aluminum foil and on carbon coated aluminum foil (CB/Al) in two different electrolytes 1M NaTf/G4 (Tetraglyme) and 1M NaPF$_6$/G2 (Figure S7). The aluminum substrates showed poor performance, with frequent drop in coulombic efficiency and unpredictable behavior. On the other hand, the carbon coating drastically improved the stability. The coulombic efficiency of plating/stripping on CB/Al during first cycle was 76.5% in G4 and 84.2% in G2. Afterward it quickly stabilized around 98.5% in G2, while it took around 15 cycles to stabilize around 98% in G4. In a full cell assembly this would translate in repeated loss of available capacity from the cathode source. These tests are in good agreement with previous literature on CB/Al in ether-based electrolyte[3]. Following this, NaPF$_6$/G2 was chosen as electrolyte. After 250 plating/stripping cycles, ex-situ digital images were acquired at the plated state (Figure S8) to highlight the different deposition of sodium on bare Al and CB/Al. It is believed that the deposition of sodium onto the Al substrate is firstly initiated in few nucleation sites and subsequently a sodium build-up on those seeds is favored, resulting in a compact deposition spot, increasing the risk of dendrites. On the other hand, CB/Al substrate allows multiple seeding thanks to the reduced energy barrier and the plated deposit result to be less centralized and more distributed.

Electrochemical Impedance Spectroscopy (EIS) was used to gain insight on the formation and the stability of SEI layer during the first crucial cycles of both Al and CB/Al substrates. The spectra reported in Figure S9, are acquired after the 1st, 2nd 3rd and 10th full cycle of plating and stripping. The overall impedance of the Al substrate is one order of magnitude higher than that of CB/Al, underlining the higher energy barrier needed to initiate plating on a bare metal substrate. Furthermore, the high frequency semicircle attributed to the SEI layer is stable over cycling for the CB/Al substrate while is becoming more prominent over cycling for Al substrate, in good agreement with what has been already reported in literature[3,25].
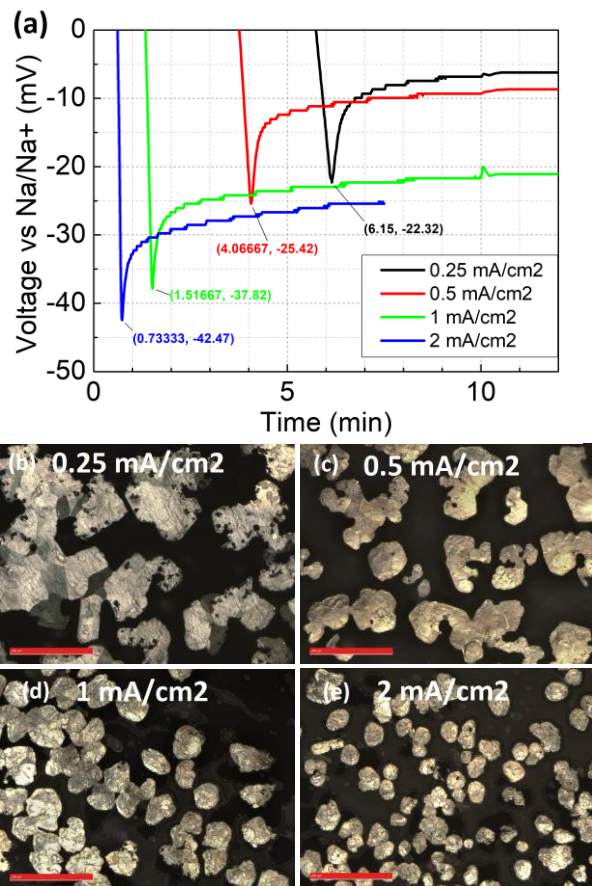

Figure 6. Comparison of nucleation overpotentials at different current rates on carbon coated aluminum substrate (a) and ex-situ optical images after the first plating cycle with 0.25 mAh/cm^2 loading of sodium, at a current rate of 0.25 (b), 0.5 (c), 1 (d) and 2 mA/cm^2 (e); scale bar 200 μm.

To gain further insight on the rate capabilities of the CB/Al substrate, plating was performed at different current rates and ex-situ optical images were acquired. The rate tested were 0.25, 0.5, 1, 2 mA/cm^2 maintaining the same sodium loading of 0.25 mAh/cm^2 (Figure 6(a)). As expected, the nucleation potential is affected by the current rate and shows a clear trend; when the plating current is increased, the overpotential increases in absolute value, going from -22 mV (at low rate 0.25 mA/cm^2) up to -42 mV (at high rate 2 mA/cm^2). Also, the average plating voltage increases accordingly giving values of -5.1, -8.6, -22.5, -27.7 mV at the currents of 0.25, 0.5, 1, 2 mA/cm^2 respectively. Further investigations on the morphology of the sodium deposits were conducted ex situ after the first plating discharge by optical imaging (Figure 6(b)-(d)). At low rate few nuclei of sodium are deposited and they form as large agglomerates suggesting the preference of particle growth over nucleation. On the other hand, at high rates the Na seeds are higher in number but smaller in size implying that nucleation is promoted over growth. Over the whole range of currents tested, no significant localized build up has been detected, granting a low risk of dendrite growth.

These results confirm that the carbon layer improves cycling stability and facilitates nucleation, which is fundamental for achieving high current rates. To prove this further, rate capability tests for CB/Al in NaPF$_6$/G2 up to 2 mA/cm^2 have al-

so been performed and low voltage hysteresis of 8, 12, 21, 40 mV can been seen at current rates of 0.25, 0.5, 1 and 2 mA/cm^2, respectively (Figure S10). A low hysteresis at high current rate will enable a low polarization during operation in full cell and no major drop is expected in cell potential, which translates in the possibility of delivering high-power.

A full cell was then assembled using Fe-HCF@rGO as cathode and the CB/Al substrate as negative electrode in NaPF$_6$/G2 electrolyte. Both electrodes were pre-treated in half-cells before assembly in full cell to overcome initial sodium deficiency, cleaning the substrate surface as well as facilitate nucleation. In particular the cathode was sodiated to its maximum sodiation state to maximize the capacity while the carbon black substrate was pre-activated with a negligible ~4μAh/cm^2 loading of sodium to maximize the first cycle efficiency.
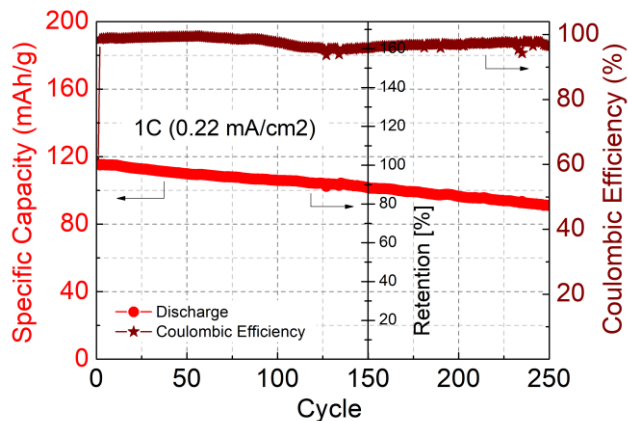

Figure 7. Long cycling performances of anode-free full cell Fe-HCF@rGO//CB/Al in 1M NaPF$_6$/G2 at 1C (150 mA/g and 0.22 mA/cm^2).

The full cell was evaluated in the voltage range 2 to 3.9 V over 250 cycles at 1C (150 mA/g) which corresponds to 0.22 mA/cm^2 (see Figure 7). It is worth highlighting that with a low Fe-HCF@rGO loading of 1.5 mg/cm^2, the sodium aerial loading on the substrate is of 0.17 mAh/cm^2.

Interesting considerations on electroplating-based LIBs have been highlighted by Albertus et al.[26] regarding the large excess of lithium metal adopted for testing high-energy cells, way more than needed, which in turns could carry to distortion of research results. The same could be said for the aerial sodium loadings often involved which are, in fact, in the range of 1 to 4 mAh/cm^2. Lowering this parameter incurs in more demanding test conditions where the initial seeding/final stripping onto the substrate play a major role, influencing the performances at full cell level. Much different is in fact the behaviour of a cell where a pre-plated negative substrate with excess sodium is used. During full cell operation, when Na metal is deposited *in situ* at the negative electrode, the amount of Na is directly related to (and limited by) the cathode host material, its weight and its maximum state of sodiation. Hence the set of electroplating tests presented is oriented to reflect the real behaviour of a finite source of sodium subjected to deep cycling. By doing this, we proved that it is possible to stabilize the plating/stripping mechanisms even when low aerial capacity loading such as 0.17 mAh/cm^2 are used (five to twenty times lower than what is often reported in literature).

Despite these challenging conditions, the full cell displayed good performances. A specific capacity of 115 mAh/g was delivered at the second cycle, 93% of which was maintained after 100 cycles, and 79% after 250 cycles, with a decline of only 0.084% per cycle, showing remarkable capacity retention. Calculating the specific energy based on the active mass of the cathode (no mass at the anode side), we reach 338 Wh/kg on the first discharge (see Figure S11), which is much higher than most SIBs full cells to date[1,27].
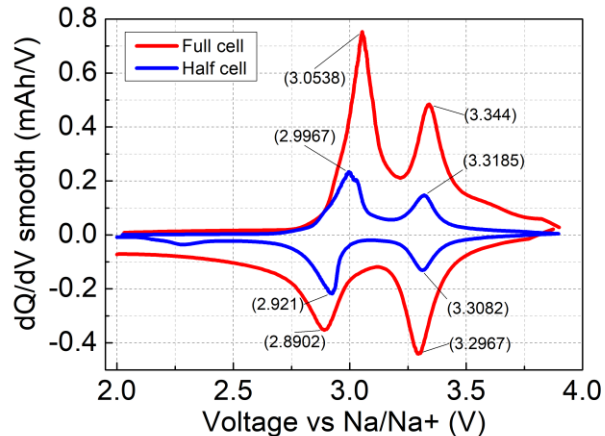

Figure 8. Voltage derivatives of the specific capacity vs voltage curve of full cell Fe-HCF@rGO//CB/Al compared to half cell Fe-HCF@rGO//Na at 1C.

To achieve a good retention, high coulombic efficiency must be maintained, and its value can be used to calculate in first approximation the lifespan of the battery[2]. During the first cycle of the full cell, the sodium is extracted from the Fe-HCF@rGO cathode and it is plated on the CB/Al. The first cycle efficiency is only 60.6% because of the conditioning of the negative substrate and the formation of the SEI on the firstly plated Na. After this initial loss of capacity, 115 mAh/g are delivered at the second cycle and an efficiency of 98.5% is promptly reached, which enable a good retention for 250 cycles.

In order to investigate the redox kinetics within the full cell, the first derivative of the charge is plotted against voltage in Figure 8, comparing half cell and full cell at 1C. The peaks corresponding to Fe$_{LS}$(C) (high potential) and Fe$_{HS}$(N) (low potential) are clearly visible in full cell as they are in half cell, meaning that full utilization of Fe-HCF is occurring. The slight shift between half cell and full cell is proportional to the polarization due to plating/stripping hysteresis onto CB/Al. From plating tests on CB/Al we expect an hysteresis of ca. 8 mV from the substrate, when the rate is 0.25 mA/cm^2. This amount is reflected in the polarization of 5 mV during oxidation and 3 mV during reduction of the Fe$_{HS}$(N) couple seen in full cell. The high voltage couple practically does not suffer any polarization.
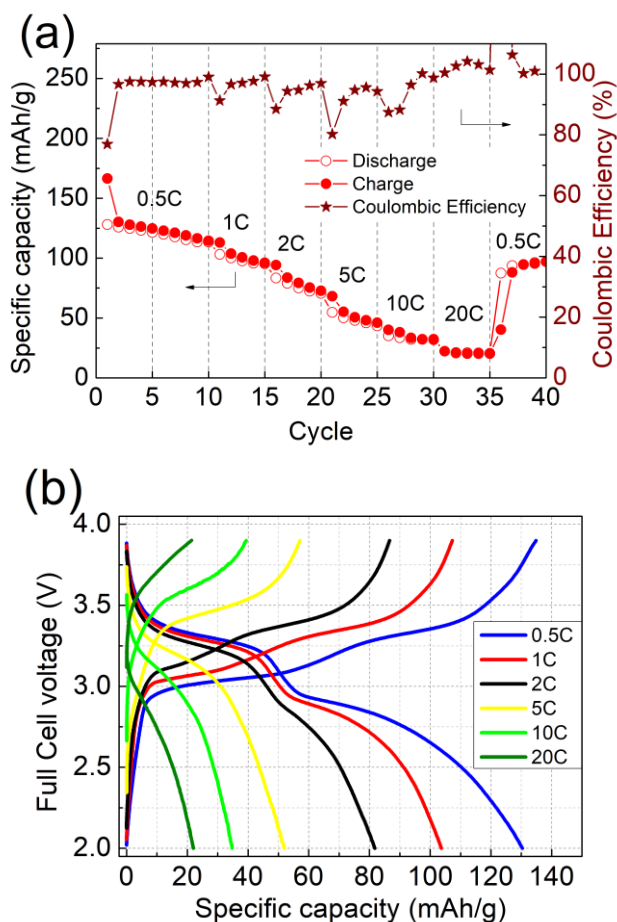
Figure 9. Waterfall plot of C-rates of full cell system (a) and discharge voltage profiles at increasing current rates (b).

Table 1. Input and output (discharge) parameters of full cell rate capability test reported in Figure 9.

C rate	0.5 C	1 C	2 C	5 C	10 C	20 C
mA/g$_{PB}$	75	150	300	750	1500	3000
mA/cm^2	0.08	0.16	0.32	0.64	1.58	3.17
mAh/g$_{PB}$	130	113	94	68	40	22
average V	2.93	2.96	2.97	2.95	2.87	2.66
W/kg$_{PB}$	248	503	1008	2501	4875	9010

Recently, diverse solutions for electroplating-based sodium-ion full cells employing a variety of cathode materials and of negative substrates were proposed. Oxides ($Na_{0.9}[Cu_{0.22}Fe_{0.30}Mn_{0.48}]O_2$[28], $Na_{0.67}Ni_{0.33}Mn_{0.67}O_2$[29], $NaNi_{0.5}Mn_{0.2}Ti_{0.3}O_2$[30]), phosphates ($Na_3V_2(PO_4)_3$[31–33], $Na-Ti_2(PO_4)_3$[34]), pyrite ($Na_{1.5}FeS_2$[3,35]) and Prussian blue[27,36] have been reported so far and their performances are briefly summarized in Table S4. Where specified, some of the tests reported in literature were performed with different charge/discharge rates to facilitate the stripping process but deviating from real world battery application.

It is worth noting the difference between an electroplating system where the negative current collector has been preloaded with Na and one which is used for *in situ* plating during operation. In most system reported in literature Na metal is galvanostatically preplated on a substrate or infused by melting process in a host material. For example in the system proposed by Lu et al.[33] a Cu current collector is firstly preloaded with 1 mAh/cm^2 of Na before being matched with a $Na_3V_2(PO_4)_3$@C cathode. Similarly, 4 mAh/cm^2 were pre-deposited on a carbon paper current collector before assembly with a Prussian Blue cathode[36]. In the same manner, 4 mAh/cm^2 were pre-plated on Graphitized Caron Microsphere substrate before assembly with an oxide cathode[30]. In another system presented by Chang et al.[32] a $Na_3V_2(PO_4)_3$ cathode is paired with an hybrid Na-MoS_2 negative electrode, which contains 60 %wt of metallic Na. Other systems presented propose a host matrix of carbon felt[29] or wood-derived electrode[37] infused with high quantities of Na. On the other hand, adopting in-situ metal plating, we achieve two advantages: we reduce the amount of sodium in the cell to a minimum hence we minimize the entity of risk represented by dendrite formation, and at the same time we avoid sensitive handling of sodium metal. Our system Fe-HCF@rGO//CB/Al was able to deliver 338 Wh/kg and 503 W/kg at 1C and still deliver 60 Wh/kg when the power drained was 9010 W/kg (20C), reaching the highest power levels reported to date for metal plating based sodium batteries.
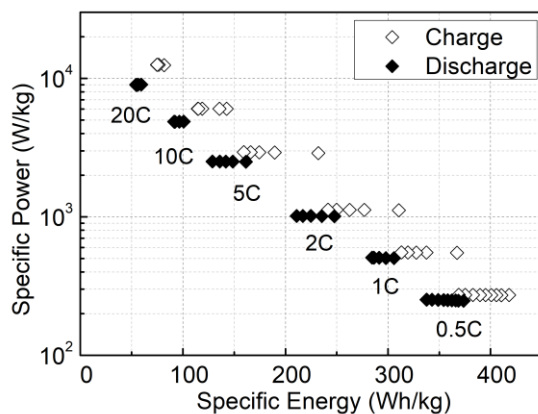
Rate capability tests (Figure 9) performed on the full cell showed that the fast kinetics at both electrodes enabled low polarization of the redox plateaus up to 2C (250 mA/g, 0.32 mA/cm^2) and it is only above 5C (750 mA/g, 0.64 mA/cm^2) that the electroplating kinetics start to mask the response of of the cathode. In Table 1 are reported the details of the current input and capacity and power output. When the current is increased ten times from 0.5 C to 5 C the full cell is still able to deliver 40% of its capacity.

Despite the fade in capacity at high rates, the high potential couple Fe$_{LS}$(C) remains predominant and the average voltage is maintained high. Hence the delivered power of this system is remarkably high and results on average: 248, 503, 1008, 2501, 4875 and 9010 W/kg when the current rates are 75, 150, 300, 750, 1500, 3000 mA/g, respectively (Figure 10). To date, these are the highest power levels reported in literature for a sodium ion full cell employing metal electroplating.

Figure 10. Representation of the anode-free full cell performances at different current rates in a Ragone plot.

Conclusions

In this work we have engineered and studied the behavior of a full Na-ion battery whose working mechanism is based on in-situ metal plating. This particular cell architecture was chosen as it allows the boosting of gravimetric capacity through the removal of the anode active material as well as enabling fast surface kinetics, opening the way to the realization of high-energy and high-power systems.

Our cell comprises a composite Prussian Blue - reduced Graphene Oxide (Fe-HCF@rGO) cathode material and a negative current collector composed of a thin layer of carbon black coated on aluminum foil (CB/Al). 1M $NaPF_6$/Diglyme is used as electrolyte.

The rGO-assisted synthesis of Fe-HCF results in a material with minimal structural defects and low water content which is fundamental for the optimization of the electrochemical performances. At the same time the presence of the rGO matrix enhances the electronic conductivity facilitating efficient response at high current rates. In fact, 69% of the capacity delivered at 0.5C is still maintained when the current rate is increased to 20C. Moreover, thanks to the low defect structure the high potential $Fe_{LS}(C)$ redox couple maintains its activity at high rates, which translate in high voltage output in full cell. At the negative electrode a highly reversible metal plating/stripping mechanism is stabilized on CB/Al substrate up to 2 mA/cm^2 with a low voltage hysteresis of 40 mV. Small stripping overpotential implies that the overall output voltage in full cell will not be reduced significantly.

By designing this high-power sodium ion battery we highlight the importance of performing testing conditions that reflect full cell application, In doing this, we demonstrate the possibility of stabilizing a small areal sodium loading (0.17 mAh/cm^2) coming from a finite cathode source. Such system reached the typical cut-off capacity retention of 80% after 250 cycles at 1C. The absence of anode active mass translates into output specific energy of 338 Wh/kg at 1C. While, thanks to the high voltage and good rate capability, the full cell reached the maximum specific power of 9010 W/kg.

Thanks to its remarkable performances, this Prussian Blue-based *in situ* metal plating battery can be located in a very interesting area of the Ragone plot overcoming the boundaries between batteries and supercapacitors. This simplified anode-free cathode-sourced architecture proved to be a highly competitive and inexpensive approach for a variety of Na-ion applications.

AUTHOR INFORMATION

Corresponding Author

* Serena Margadonna: s.margadonna@swansea.ac.uk

* Francesco Mazzali: francesco.mazzali@swansea.ac.uk

Author Contributions

All authors have given approval to the final version of the manuscript.

ABBREVIATIONS

Fe-HCF = Iron Hexacyanoferrate;
Fe-HCF@rGO = Iron Hexacyanoferrate – reduced Graphene Oxide composite;
G2 = Diglyme;
G4 = Tetraglyme;
CB/Al = Carbon Black coated Aluminum.

REFERENCES

(1)   Dubal, D. P.; Ayyad, O.; Ruiz, V.; Gómez-Romero, P. Hybrid Energy Storage: The Merging of Battery and Supercapacitor Chemistries. *Chem. Soc. Rev.* **2015**, *44*, 1777–1790.

(2)   Qian, J.; Adams, B. D.; Zheng, J.; Xu, W.; Henderson, W. A.; Wang, J.; Bowden, M. E.; Xu, S.; Hu, J.; Zhang, J. G. Anode-Free Rechargeable Lithium Metal Batteries. *Adv. Funct. Mater.* **2016**, *26*, 7094–7102.

(3)   Cohn, A. P.; Muralidharan, N.; Carter, R.; Share, K.; Pint, C. L. Anode-Free Sodium Battery through in Situ Plating of Sodium Metal. *Nano Lett.* **2017**, *17*, 1296–1301.

(4)   Irisarri, E.; Ponrouch, A.; Palacin, M. R. Review—Hard Carbon Negative Electrode Materials for Sodium-Ion Batteries. *J. Electrochem. Soc.* **2015**, *162*, A2476–A2482.

(5)   Qian, J.; Wu, C.; Cao, Y.; Ma, Z.; Huang, Y.; Ai, X. Prussian Blue Cathode Materials for Sodium-Ion Batteries and Other Ion Batteries. *Adv. Energy Mater.* **2018**, *1702619*, 1–24.

(6)   Chen, R.; Huang, Y.; Xie, M.; Zhang, Q.; Zhang, X.; Li, L.; Wu, F. Preparation of Prussian Blue Submicron Particles with a Pore Structure by Two-Step Optimization for Na-Ion Battery Cathodes. *ACS Appl. Mater. Interfaces* **2016**, *8*, 16078–16086.

(7)   Wu, X.; Deng, W.; Qian, J.; Cao, Y.; Ai, X.; Yang, H. Single-Crystal FeFe(CN)6 Nanoparticles: A High Capacity and High Rate Cathode for Na-Ion Batteries. *J. Mater. Chem. A* **2013**, *1*, 10130–10134.

(8)   Yang, D.; Xu, J.; Liao, X. Z.; Wang, H.; He, Y. S.; Ma, Z. F. Prussian Blue without Coordinated Water as a Superior Cathode for Sodium-Ion Batteries. *Chem. Commun.* **2015**, *51*, 8181–8184.

(9)   Wang, H.; Wang, L.; Chen, S.; Li, G.; Quan, J.; Xu, E.; Song, L.; Jiang, Y. Crystallographic-Plane Tuned Prussian-Blue Wrapped with RGO: A High-Capacity, Long-Life Cathode for Sodium-Ion Batteries. *J. Mater. Chem. A* **2017**, *5*, 3569–3577.

(10)   Prabakar, S. J. R.; Jeong, J.; Pyo, M. Highly Crystalline Prussian Blue/Graphene Composites for High-Rate Performance Cathodes in Na-Ion Batteries. *RSC Adv.* **2015**, *5*, 37545–37552.

(11)   Jiang, Y.; Yu, S.; Wang, B.; Li, Y.; Sun, W.; Lu, Y.; Yan, M.; Song, B.; Dou, S. Prussian Blue@C Composite as an Ultrahigh-Rate and Long-Life Sodium-Ion Battery Cathode. *Adv. Funct. Mater.* **2016**, *26*, 5315–5321.

(12)   You, Y.; Yao, H. R.; Xin, S.; Yin, Y. X.; Zuo, T. T.; Yang, C. P.; Guo, Y. G.; Cui, Y.; Wan, L. J.; Goodenough, J. B. Subzero-Temperature Cathode for a Sodium-Ion Battery. *Adv. Mater.* **2016**, 7243–7248.

(13)   Tang, Y.; Zhang, W.; Xue, L.; Ding, X.; Wang, T.; Liu, X.; Liu, J.; Li, X.; Huang, Y. Polypyrrole-Promoted Superior Cyclability and Rate Capability of NaxFe[Fe(CN)6] Cathodes for Sodium-Ion Batteries. *J. Mater. Chem. A* **2016**, *4*, 6036–6041.

(14)   Seh, Z. W.; Sun, J.; Sun, Y.; Cui, Y. A Highly Reversible Room-Temperature Sodium Metal Anode. *ACS Cent. Sci.* **2015**, *1*, 449–455.

(15)   Robin, M. B.; Day, P. Mixed Valence Chemistry - A Survey and Classification. *Adv. Inorg. Chem. Radiochem.* **1967**, *10*, 247–422.

(16)   Piernas Muñoz, M. J.; Castillo Martínez, E. *Prussian Blue Based Batteries*, SpringerBr.; Springer, Ed.; Springer, Cham, 2018.

(17)   Wu, X.; Shao, M.; Wu, C.; Qian, J.; Cao, Y.; Ai, X.; Yang, H. Low Defect FeFe(CN)6 Framework as Stable Host Material for High Performance Li-Ion Batteries. *ACS Appl. Mater. Interfaces* **2016**, *8*, 23706–23712.

(18)   Rudola, A.; Du, K.; Balaya, P. Monoclinic Sodium Iron Hexacyanoferrate Cathode and Non-Flammable Glyme-Based Electrolyte for Inexpensive Sodium-Ion Batteries. *J. Electrochem. Soc.* **2017**, *164*, A1098–A1109.

(19)   Westman, K.; Dugas, R.; Jankowski, P.; Wieczorek, W.; Gachot, G.; Morcrette, M.; Irisarri, E.; Ponrouch, A.; Palacín, M. R.; Tarascon, J.-M. Diglyme Based Electrolytes for Sodium-Ion Batteries. *ACS Appl. Energy Mater.* **2018**, *1*, 2671–2680.

(20)   Luo, J.; Sun, S.; Peng, J.; Liu, B.; Huang, Y.; Wang, K.; Zhang, Q.; Li, Y.; Jin, Y.; Liu, Y. Graphene-Roll-Wrapped Prussian Blue Nanospheres as a High-Performance Binder-Free Cathode for Sodium-Ion Batteries. *ACS Appl. Mater. Interfaces* **2017**, *9*, 25317–25322.

(21)   Wang, L.; Song, J.; Qiao, R.; Wray, L. A.; Hossain, M. A.; Chuang, Y. De; Yang, W.; Lu, Y.; Evans, D.; Lee, J. J. Rhombohedral Prussian White as Cathode for Rechargeable Sodium-Ion Batteries. *J. Am. Chem. Soc.* **2015**, *137*, 2548–2554.

(22)   Ai, W.; Du, Z.; Fan, Z.; Jiang, J.; Wang, Y.; Zhang, H.; Xie, L.; Huang, W.; Yu, T. Chemically Engineered Graphene Oxide as High Performance Cathode Materials for Li-Ion Batteries. *Carbon N. Y.* **2014**, *76*, 148–154.

(23)   Xiong, D.; Li, X.; Shan, H.; Zhao, Y.; Dong, L.; Xu, H.; Zhang, X.; Li, D.; Sun, X. Oxygen-Containing Functional Groups Enhancing Electrochemical Performance of Porous Reduced Graphene Oxide Cathode in Lithium Ion Batteries. *Electrochim. Acta* **2015**, *174*, 762–769.

(24)   Yan, C.; Zhang, Z.; Liu, Z.; Liu, Y.; Wu, S. Excellent Long-Term Electrochemical Performance of Graphite Oxide as Cathode Materials for Lithium-Ion Batteries. *Ionics (Kiel).* **2017**, *23*, 3023–3029.

(25)   Liu, S.; Tang, S.; Zhang, X.; Wang, A.; Yang, Q. H.; Luo, J. Porous Al Current Collector for Dendrite-Free Na Metal Anodes. *Nano Lett.* **2017**, *17*, 5862–5868.

(26)   Albertus, P.; Babinec, S.; Litzelman, S.; Newman, A.; Albertus, P.; Babinec, S.; Litzelman, S.; Newman, A. Status and Challenges in Enabling the Lithium Metal Electrode for High-Energy and Low-Cost Rechargeable Batteries. *Nat. Energy* **2018**, *3*, 16–21.

(27)   Rudola, A.; Gajjela, S. R.; Balaya, P. High Energy Density In-Situ Sodium Plated Battery with Current Collector Foil as Anode. *Electrochem. commun.* **2018**, *86*, 157–160.

(28)   Wei, L.; Chuan- Fu, L.; Oliver, Z.; Malachi, N.; Ying, Z.; W., R. G.; Liangbing, H.; Luo, W.; Lin, C.; Zhao, O. Ultrathin Surface Coating Enables the Stable Sodium Metal Anode. *Adv. Energy Mater.* **2016**, *7*, 1601526.

(29)   Chi, S. Sen; Qi, X. G.; Hu, Y. S.; Fan, L. Z. 3D Flexible Carbon Felt Host for Highly Stable Sodium Metal Anodes. *Adv. Energy Mater.* **2018**, *8*, 1702764.

(30)   Ye, H.; Wang, C. Y.; Zuo, T. T.; Wang, P. F.; Yin, Y. X.; Zheng, Z. J.; Wang, P.; Cheng, J.; Cao, F. F.; Guo, Y. G. Realizing a Highly Stable Sodium Battery with Dendrite-Free Sodium Metal Composite Anodes and O3-Type Cathodes. *Nano Energy* **2018**, *48*, 369–376.

(31)   Cao, R.; Mishra, K.; Li, X.; Qian, J.; Engelhard, M. H.; Bowden, M. E.; Han, K. S.; Mueller, K. T.; Henderson, W. A.; Zhang, J. G. Enabling Room Temperature Sodium Metal Batteries. *Nano Energy* **2016**, *30*, 825–830.

(32)   Zhang, D.; Li, B.; Wang, S.; Yang, S. Simultaneous Formation of Artificial SEI Film and 3D Host for Stable Metallic Sodium Anodes. *ACS Appl. Mater. Interfaces* **2017**, *9*, 40265–40272.

(33)   Lu, Y.; Zhang, Q.; Han, M.; Chen, J. Stable Na Plating/Stripping Electrochemistry Realized by a 3D Cu Current Collector with Thin Nanowires. *Chem. Commun.* **2017**, *53*, 12910–12913.

(34)   Zhou, W.; Li, Y.; Xin, S.; Goodenough, J. B. Rechargeable Sodium All-Solid-State Battery. *ACS Cent. Sci.* **2017**, *3*, 52–57.

(35)   Tang, S.; Qiu, Z.; Wang, X. Y.; Gu, Y.; Zhang, X. G.; Wang, W. W.; Yan, J. W.; Zheng, M. Sen; Dong, Q. F.; Mao, B. W. A Room-Temperature Sodium Metal Anode Enabled by a Sodiophilic Layer. *Nano Energy* **2018**, *48*, 101–106.

(36)   Zhang, Q.; Lu, Y.; Zhou, M.; Liang, J.; Tao, Z.; Chen, J. Achieving a Stable Na Metal Anode with a 3D Carbon Fibre Scaffold. *Inorg. Chem. Front.* **2018**, *5*, 864–869.

(37)   Luo, W.; Zhang, Y.; Xu, S.; Dai, J.; Hitz, E.; Li, Y.; Yang, C.; Chen, C.; Liu, B.; Hu, L. Encapsulation of Metallic Na in an Electrically Conductive Host with Porous Channels as a Highly Stable Na Metal Anode. *Nano Lett.* **2017**, *17*, 3792–3797.

Graphical abstract for TOC